analytical chemistry

Article

Cite This: Anal. Chem. 2019, 91, 2876−2884

pubs.acs.org/ac

Magnetic Focus Lateral Flow Sensor for Detection of Cervical Cancer Biomarkers

Wen Ren,[†] Sulma I. Mohammed,[‡] Steven Wereley,[§] and Joseph Irudayaraj*[,†]

[†]Bioengineering, Cancer Center at Illinois, University of Illinois at Urbana−Champaign, Urbana, Illinois 61801, United States

[‡]College of Veterinary Medicine and [§]School of Mechanical Engineering, Purdue University, West Lafayette, Indiana 47907, United States

Supporting Information

ABSTRACT: We report on a magnetic focus lateral flow biosensor (mLFS) for ultrasensitive detection of protein biomarkers in a practical format. With valosin-containing protein as a target protein, we show that the developed mLFS concept could detect as low as 25 fg/mL with magnetic focus to enhance target capture efficiency to deliver a 10^6-fold improvement in sensitivity compared to that of conventional lateral flow (LF) systems. The conceptualized strategy utilizes a simple magnet placed beneath the three-dimensional printed LF device to concentrate the targets at the signal zone without any additional instrumentation. In addition, protein mixtures extracted from the tissue of cervical cancer patients was also utilized to validate the sensor. To investigate the effect of magnetic focus on sensitivity, surface-enhanced Raman spectroscopy and dark-field imaging was utilized to characterize the distribution and movement of Fe_3O_4 core−Au shell nanoprobes in a model LF strip. Our experiments show that the magnetic focus results in an increased interaction time between the magnetic probe-labeled targets and the capture antibody, yielding a higher capture efficiency, allowing for ultrasensitive detection of the target not possible before with LF. The proposed mLFS can be utilized to detect a range of trace protein biomarkers for early diagnosis and can be combined with diverse pretreatment and signal amplification steps to query complex samples.

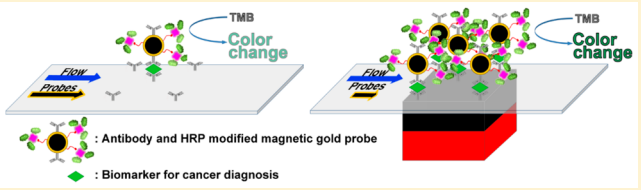

Short detection time, on-site operation, and versatility are salient features of the lateral flow immunoassay (LFIA), making it an ideal tool for point-of-care (POC) tests. LFIA has been used to detect diverse protein targets, viruses, and pathogenic bacteria.[1−6] With integration of multiple antibodies against different targets on a single strip, LFIA has also been used for target screening.[7,8] The lateral flow (LF) strips comprise several pieces of paper-based material assembled on a plastic backboard, making LFIA a cost-effective technique. The porous paper-based material provides a conducive environment for target capture with signal amplification steps.[3,9] With this simple technique, complex matrixes such as blood, urine, and even food matrixes or unpurified water samples were analyzed.[3,4,10−13] The LF strip has been fitted with a portable reader or a smartphone accessory for on-site application.[14,15] LFIA has already exhibited strong commercial success for instance as a pregnancy test kit with an estimated market value of about 4.7 billion U.S. dollars worldwide as of 2015.[16]

Although LFIA is a promising analytical technique, primary limitation is its lack of sensitivity to detect targets at low levels while retaining its simplicity. For instance, with conventional LFIA the sensitivity for protein detection has been reported to be in microgram per milliliter,[17] whereas the expectation for POC tests and other applications require a much higher sensitivity. One possible route for improved sensitivity is sample pretreatment for target concentration, which could also reduce the influence from the nontarget substances when using complex samples and mixtures.[4,18,19] Pretreatment to process different samples with LFIA requires additional instrumentation and increased detection time. Another common strategy is to prepare probes with nanoparticles with high extinction coefficient such as gold or silver nanoparticles that can provide a strong colorimetric readout[20,21] for further enhancement with silver staining to improve the visible signal.[9,22] Fluorescent signals using florescent beacons such as nanoparticles doped with fluorophore molecules, quantum dots, and upconversion nanoparticles could provide improved sensitivity compared to colorimetric signals,[1,23,24] but they require a fluorescent reader. Besides, enzyme-based colorimetric signal amplification has also been used to further improve LFIA.[3]

From past work, one of the compounding factors that affect sensitivity of LFIA is the capture efficiency of targets at the detection (or target capture) zone. This in fact is influenced by the flow speed of the sample in the LF strip, which also affects the binding kinetics (due to less interaction time) of the targets in the sample at the capture zone. For instance, Zeng et al. constructed LF strips with two types of nitrocellulose (NC) membranes with a 3 and 4 min sample migration time to yield a signal-to-noise ratio of 13 and 11, respectively, indicating slightly improved results from the strips with longer sample migration

Received: October 23, 2018
Accepted: January 11, 2019
Published: January 11, 2019

DOI: 10.1021/acs.analchem.8b04848
Anal. Chem. 2019, 91, 2876−2884

times.[25] Kumar et al. assembled LF strips with NC membranes of pore size 5, 10, and 15 μm and showed that 5 μm pore size yielded better sensitivity because it had the slowest wicking time.[26] The relationship between sensitivity and duration of flow (i.e., flow speed) on the NC membrane was attributed to the interaction time: the longer the flow time, the longer the interaction time of the probe-labeled targets with the antibodies immobilized at the detection zone, resulting in a higher target capture efficiency and thus better sensitivity.[17] It should be noted that in an LF strip the sample migration on the strip depends on capillary action, so as to present the targets to the probes located at the conjugate pad for labeling and to the antibodies immobilized at the detection zone for recognition. These initial efforts demonstrated that by reducing the rate at which the sample flows on the strip, the interaction time of the target and the capture antibodies can be increased, allowing for a higher capture efficiency. Several strategies were proposed based on this concept. For instance, Rivas et al. printed wax pillars of different patterns on the LF strip to give rise to a pseudoturbulence flow effect, yielding a slight improvement in sensitivity.[27] Tang et al. added a sponge between conjugate pad and NC membrane to reduce the fluid flow rate, to achieve a tenfold signal improvement.[28] An electrophoresis technique termed as isotachophoresis (ITP) was introduced to regulate the movement of charged probes in the strip controlled by voltage.[29−31] However, ITP-based LFIA methods require extra instrumentation and experimental setup for voltage control to regulate the flow of probes.

Herein, we propose a unique strategy termed as magnetic focus lateral flow sensor (mLFS) whereby a simple low-cost magnet is utilized to increase the residence time of the target labeled with gold-coated magnetic probes at the detection zone. The magnetic probes comprise Fe_3O_4 core/gold shell nanostructures modified with antibodies for target recognition and an enzyme-based colorimetric signal amplification. The magnetic focus concept could control the movement of probe-labeled target in the LF strip because of the magnetic field provided by a simple external magnet placed under the LF strip. The sensitivity obtained could be increased more than 10^6 times assisted by an enzyme-based amplification compared to the conventional LFIA system for protein detection[32,33] or 2×10^4 times compared to the current enhanced techniques reported in the literature.[34] We have utilized this strategy for pathogen detection with two probes, magnetic probe for magnetic focus to enhance target capture efficiency and gold probes for enzymatic amplification.[35] Although excellent sensitivity was obtained, the improvement in sensitivity is limited because of the size of the bacterial cells (1−3 μm) and its control by the magnetic force.

In our previous research, the relation between expression level of valosin-containing protein (VCP) and cervical cancer was demonstrated.[36] Here, we develop an ultrasensitive platform to detect VCP. With magnetic focus, as low as 25 fg/mL of purified VCP could be detected in phosphate buffered saline (PBS) buffer with naked eyes within 45 min assisted by enzyme-based colorimetric signal amplification. To the best of our knowledge, this is the lowest detected protein level reported by visual recognition utilizing LF devices. Contrastingly, without magnetic focus, as high as 100 pg/mL of VCP could not give rise to any visible signal in control experiments when other detection conditions are the same with enzymatic amplification. When real samples were tested, in extracted protein mixture from tissue lysates, VCP can be recognized in 16 pg/mL of total protein, suggesting the detection of VCP in low amounts from tissue samples.

To further understand mLFS, for the first time we show evidence of the contribution of magnetic focus on enhanced sensitivity by surface-enhanced Raman spectroscopy (SERS) and dark-field imaging of the modified magnetic nanoparticles along with particle image velocimetry (PIV) experiment. With an external magnet, in a simulated system we note from the SERS intensity change and dark-field images a higher concentration of probes at the target zone. Furthermore, PIV analysis of dark-field images indicated a slower speed, affirming increased interaction time. The spatial distribution of probes along the cross-section of a microchannel was also evaluated. Results indicate a higher concentration of targets at the signal generation zone, contributing to increased capture efficiency, resulting in improved sensitivity.

EXPERIMENTAL SECTION

Materials. $HAuCl_4{\cdot}xH_2O$, $FeCl_3$, $FeCl_2$, 4-mercaptopyridine (4-MPy), sodium citrate, and sodium carbonate reagents were obtained from Sigma (St. Louis, MO, U.S.A.). NaOH was purchased from Mallinckrodt Chemicals (Bedminster, NJ, U.S.A.). $NaBH_4$ was obtained from Acros Organics (Morris Plains, NJ, U.S.A.). Tetramethyl benzidine (TMB) substrate solution was obtained from Moss Inc. (Hanover, MD, U.S.A.). Purified VCP (catalog number: CF48) was obtained from Novoprotein (Summit, NJ, U.S.A.). The anti-VCP antibodies p97/VCP antibody (2H5) (M15) and p97/VCP antibody (2B2) (M18) were purchased from Novus Biologicals, LLC (Centennial, CO, U.S.A.). Pierce Streptavidin Poly-HRP (HRP, horseradish peroxidase) and EZ-Link Sulfo-NHS-LC-Biotin was obtained from ThermoFisher Scientific (New York, U.S.A.). All materials in the experiments were used as purchased without further purification. Glasswares used in the experiment were washed with fresh aqua regia and then rinsed with deionized (DI) water multiple times.

Probe Preparation. Magnetic probes were prepared with Fe_3O_4 core/Au shell nanostructures based on the reported method with modification.[37,38] Briefly, 30 mL of 0.1 M NaOH solution was boiled. After injection of 2 mL of 0.4 M sodium citrate solution, under strong stirring, 0.2 M $FeCl_2$ and $FeCl_3$ were quickly added. The obtained solution was refluxed for 4 h. The synthesized Fe_3O_4 was washed with ethanol and DI water three times, individually, and redispersed in 10 mL of DI water. The magnetic Fe_3O_4 core/Au shell nanoparticles were synthesized based on a quick reduction process with $NaBH_4$.[39] In general, 80 μL of Fe_3O_4 was mixed with 920 μL of DI water, followed by the addition of 100 μL of 1% $HAuCl_4$. The obtained mixture was sonicated for 15 min, and then 200 μL of 10 mM ice-cold fresh $NaBH_4$ was quickly injected. The resulting solution was sonicated for 15 min. The obtained dark red Fe_3O_4 core/Au shell nanoparticles were washed with water three times and kept at 4 °C. The nanoparticles obtained had an average diameter of about 45 nm.

The magnetic Fe_3O_4 core/Au shell nanoparticles were functionalized with biotin and antibody to recognize the target protein VCP.[3,35] One milliliter of nanoparticles was mixed with 1 μL of 0.5 M sodium carbonate and 100 μL of 10 mM phosphate buffer (pH 7.4). Then 10 μg of M18 antibody was added to the solution and shaken for 2 h. The number of antibodies bound to each nanoparticle is estimated to be around 184 by Bradford protein assay based on the change in antibody concentration before and after conjugation, and the concen-

DOI: 10.1021/acs.analchem.8b04848
Anal. Chem. 2019, 91, 2876−2884

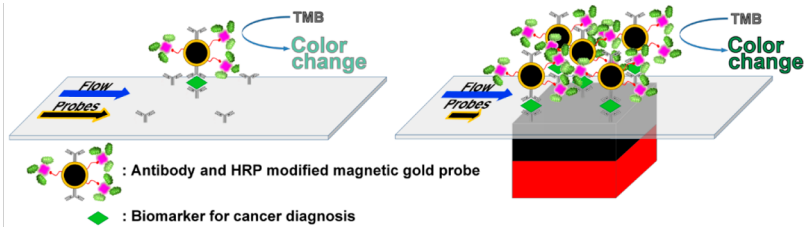

Figure 1. Schematic depicting the effect of magnetic focus in mLFS. Without magnet, the magnetic probe-labeled targets move along with the sample flow on the LF strip, resulting in a low capture efficiency (left). With magnet, the probe-labeled targets are focused at the signal generation zone due to magnetic focus, thus increasing capture efficiency of labeled targets (right).

tration of nanoparticles were determined with a prior reported method.[40] To block the residual surface of nanoparticles, 122 μL of 5% casein in 10 mM phosphate buffer was added and kept under gentle shaking overnight. With centrifugation, unbound antibodies and casein were removed and the obtained nanoparticles were redispersed in 1 mL of 10 mM phosphate buffer. To biotinylate the nanoparticles modified with antibody, 10 μg of Sulfo-NHS-LC-Biotin was added and the mixture was kept under gentle shaking for 1 h. The modified nanoparticles were washed and redispersed in 100 μL of 10 mM PBS and kept at 4 °C for detection.

Lateral Flow Strip Assembly. The lateral flow strips used in the experiments were 6.0 × 0.5 cm in size and assembled on plastic backing cards (mdi Membrane Technologies, Harrisburg, PA, U.S.A.). The strip consists of four parts: nitrocellulose membrane (90CNPH-N-SS40 from mdi Membrane Technologies) at 2.5 × 0.5 cm; absorbent pad (Grade 17 Chr Cellulose Chromatography Papers from GE Healthcare Life Sciences, Marlborough, MA, U.S.A.) at 1.5 cm × 0.5 cm; conjugate pad (Grade 6613H from Ahlstrom North America, Alpharetta, GA, U.S.A.) at 1.1 × 0.5 cm; and sample pad (Sample Pad Type GFB-R4 from mdi Membrane Technologies) at 1.7 × 0.5 cm. The NC membrane was first attached to the plastic backing card at the 1.3 cm position from one end where the absorbent pad was then attached. From the other side of the NC membrane, conjugate pad and sample pad are attached. There is a 0.2 cm overlap between each part.

Fresh-frozen tissues were obtained from Grady Hospital, Atlanta, GA, and Indiana University School of Medicine, Indianapolis, IN (sample collection and handling were performed under the approval of Emory University, Indiana University, and Purdue University Institutional Review Boards and the extraction of proteins was performed as described in a previous work.[36] The extracted proteins were transferred from the lysis buffer to PBS buffer through a trichloroacetic acid protein precipitation process, and the resulting protein pellet was dissolved in 10 mM PBS. The total concentration of the obtained protein mixture from tissue was determined with Pierce BCA protein assay kit (catalog number: 23225; ThermoFisher Scientific).

Protein Biomarker Detection. To conjugate antibodies (M15) to LF strips, 0.33 μg of M15 antibody (PBS solution) was transferred to each LF strip and then dried at 37 °C for 1 h. The obtained LF strip was placed in a three-dimensional (3D) printed device where an external magnet (N52 rare-earth neodymium permanent super strong magnet) was fixed under the strip.

The as-prepared probes were mixed with 100 μL of liquid sample as well as 10 μg/mL streptavidin poly-HRP. The obtained mixture was kept stable for 10 min to have the probes react with the VCP target. Then it is loaded on the sample pad of the LF strip and the sample was allowed to flow for 15 min. The LF strip was washed with 60 μL of DI water twice with an additional conjugate pad and absorbent pad in the cross direction every 5 min. The wash step could remove the unbound magnetic probes to avoid possible dots from blank signal for recognition with naked eyes and better sensitivity. Sixty microliters of TMB substrate was applied for the generation of colorimetric signal upon incubation at room temperature for 5 min. The LF strip was then washed with 60 μL of DI water. Images were taken to record the final results and the analysis was performed with ImageJ (National Institutes of Health, Washington, DC, U.S.A.). After normalization of images, the quantified results were obtained from the gray scale value of the part with deepest color at the dot with the average gray scale value of the blank part of the strip subtracted. Error bars represent the deviation of the colorimetric results from three replications.

PIV Analysis and Simulation on the Spatial Distribution. Volume illumination was used in particle image velocimetry (PIV) analysis. Since the particle image size, intensity, and shape vary with distance from the focal plane, even for a monodisperse suspension of particles, a Gaussian function was used to approximate the intensity distribution of particle images. This Gaussian function was used to fit each particle image to obtain the key parameters which describe particle characteristics: the peak intensity of the particle image, peak location (μx, μy), and particle diameter.[41] After each particle image was detected and fitted with the Gaussian function, the particle image is removed from the original image and the detection and analysis of the next particle occurs. The peak intensity of a particle image generally decreases and the width of it increases as the distance from the focal plane increases.[42] From the location of the detected particles, the particle concentration can be extracted. The velocity is calculated using the cross-correlation methods with the EDPIV software (developed by Dr. Lichuan Gui). EDPIV is an advanced PIV processing software package optimized for μPIV. In a steady flow such as this, averaging the correlation functions can reduce the influence of Brownian motion because Brownian motion is a zero mean normally distributed process. In our case, the correlation functions from 100 pairs of images were averaged to smooth out the effects due to Brownian motion.[43] The spatial distribution of nanoparticles in the microchannel was simulated on the basis of the results from PIV analysis. The speed distribution of nanoparticles without magnet reveals the fluid velocity profiles of the sample solution in the microchannel based on Poiseuille's law. Furthermore, because the aqua sample solution has no interaction with external magnet, the solution flow in the magnetic field should be the same compared to that without magnet. On the basis of the fluid velocity profile of sample solution, the spatial distribution of nanoparticles in the

DOI: 10.1021/acs.analchem.8b04848
Anal. Chem. 2019, 91, 2876−2884

magnetic field or without magnet in the microchannel could be determined based on the movement speed of the nanoparticles.

Characterization. UV−vis spectra of the nanoparticles and probes were recorded with a Jasco V570 UV/visible/near infrared (NIR) spectrophotometer (Jasco, Inc.). Zeta potential measurement was conducted with a Zetasizer NanoZS (Malvern Instruments). Transmission electron microscopy images of the samples were collected with a FEI Tecnai G2 20 operating at 100 kV. Raman measurement was performed with a SENTERRA confocal Raman system (Bruker Optics) with 20× long working distance objective and 785 nm excitation. Dark-field images were obtained with a 40× objective with a home-built hyperspectral dark-field imaging system.[44,45]

RESULTS AND DISCUSSION

The unsatisfactory low detection sensitivity of LFIA is one of the primary limitations of its applicability to detect trace levels of targets. Herein, we proposed a magnetic focus strategy which could significantly improve detection sensitivity of LFIA while retaining its simplicity and practicality. The concept of mLFS is illustrated in Figure 1. To generate a signal, the probe-labeled targets should be captured by the antibodies immobilized on the LF strip at the detection zone. Our goal is to increase the sensitivity by enhancing capture efficiency. The basic concept of the proposed mLFS is to improve the capture efficiency with magnetic focus provided by a simple magnet to regulate the flow behavior of magnetic probe-labeled targets after the sample is applied onto an LF strip. With use of this concept, the speed and spatial distribution of the Fe_3O_4/Au probe-labeled targets were favorably directed by the external magnetic field to result in improved capture efficiency in our design. It should also be noted that when the movement is slowed down, the interaction time of the magnetic probe-labeled targets and the capture antibodies at the detection zone is also increased. This results in a higher number of targets at the detection zone. To achieve the best magnetic focus effect, a simple frame to combine LF strip, magnet, and sample application was designed and 3D-printed. As shown in Figure 2, a small holder was used to fix the external

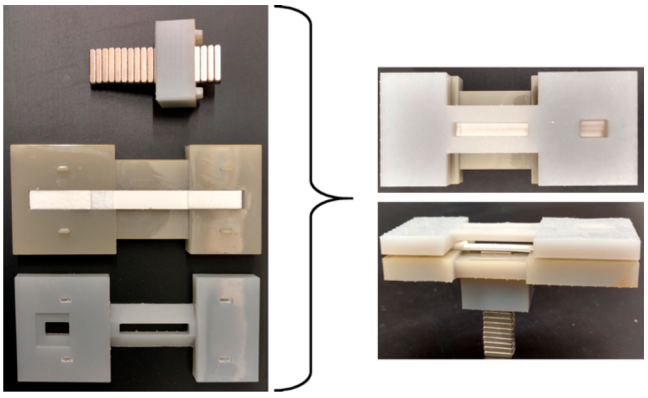

Figure 2. Sample 3D-printed kit for mLFS.

magnet just below the LF strip, a substrate with groove was used to posit the LF strip, and a cover has two windows: the smaller one for sample application and the larger one for observation of colorimetric results. The preparation of the strip and the detection procedure of mLFS was similar to that in conventional LFIA. With the implemented steps naked eye observation of color signals depicting ultralow concentration of the targets was possible without any extra instrumentation. The process can be completed in ∼45 min.

To demonstrate the modification of magnetic nanoparticles and capture of target VCP molecules, zeta potential values of the magnetic nanoparticles, antibody-modified magnetic probes, and probes capturing the target VCP were recorded. As shown in Table 1, the magnetic nanoparticles modification with antibody had an increase in the zeta potential value from −29.7 ± 1.6 to −21.2 ± 1.6 mV. The reduction of zeta potential values of the magnetic probes was noted from −21.2 ± 1.6 to −27.2 ± 2.1 mV after interaction with VCP. Since the isoelectric point of VCP is 5.14, the reduction of zeta potential was attributed to the labeling of magnetic probes with negatively charged VCP molecules in PBS solution (pH 7.4).

Table 1. Zeta Potential Measurement Conducted at 25°C

	unmodified magnetic NPs	magnetic probes	magnetic probes capturing the target VCP
zeta potential (mV)	−29.7 ± 1.6	−21.2 ± 1.6	−27.2 ± 2.1

To achieve the best sensitivity, the amount of HRP and nanoprobe was optimized and the results are shown in Figure S1 (Supporting Information) and Figure 3. Figure S1 shows typical images of detection results from serial amount of HRP. It can been seen that with more HRP the signal from the target increased while a dot from the blank could also be noted. We noted that the amount of added magnetic nanoprobes could influence the signal from the blank and 100 fg/mL of VCP in 10 mM PBS, and the results were quantified in Figure 3. For detection, the unreacted HRP in the detection zone generated a light green color in the detection zone as background, while the brightness difference between the pictures would cause a deviation in the quantified gray scale value of the strips, both of which will provide a non-zero value from the blank sample even though a dot is not produced on the LF strip. In Figure 3, it can be seen that, for the sample of 100 fg/mL VCP, the signal increased in proportion to the probes, which should be attributed to the labeling efficiency between probes and target VCP. There is no significant increase in the signal with 100 fg/mL of VCP when the probe amount was from 2 to 3 μL, which may be due to saturated labels at such low concentration of VCP. Meanwhile, although no dot was observed on the strips from the blank sample, the color from the green background became stronger with an increase in the amount of probes from 1 to 2 μL,

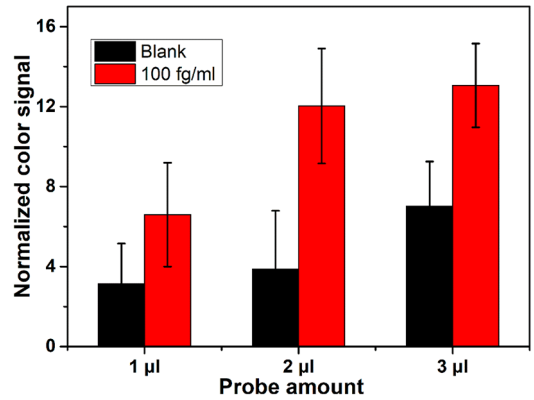

Figure 3. Probe optimization for mLFS platform.

DOI: 10.1021/acs.analchem.8b04848
Anal. Chem. 2019, 91, 2876−2884

which could be attributed to the increased amount of magnetic probes linked with HRP kept in the detection zone because of the magnetic focus. More interestingly, when 3 μL of probes was added for detection, blue-green dots were observed on the strip from the blank sample with the normalized color signal around 8. A key factor in the results is that because of the magnetic focus, the magnetic particles, irrespective of its interaction with the target, are kept in the magnetic field at the detection zone. For magnetic probes labeled with VCP, this suggests a longer interaction time between the probe-labeled VCP and antibodies immobilized at the detection zone to yield an enhanced signal of the targets. If the concentration of the unreacted probes is high, an increase in nonspecific binding of probes at the detection zone after wash gives the greenish blue color. These results indicate that the amount of magnetic probe is important for the detection sensitivity of mLFS.

To further demonstrate the magnetic focus effect of the sensor, detection of a serial concentration of VCP with and without magnet were performed while other conditions were kept the same with the optimized concentration of probes and HRP. Images of the detection results are presented in Figure 4.

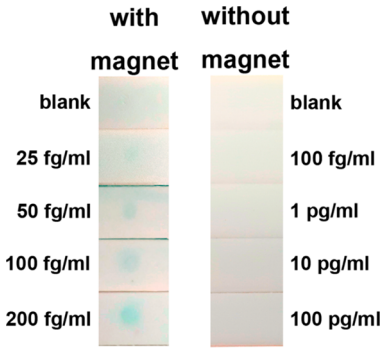

Figure 4. Comparison of detection results with and without magnet.

The presence of target VCP was determined by the appearance of a green dot in the detection zone of the strip. It can be seen that, with the magnet, a dot in light green could be observed for a concentration as low as 25 fg/mL of VCP in PBS, while on the strip from the blank no dot was observed. To the best of our knowledge, this is the lowest detected concentration of protein target to date. The color of the dots became stronger when the VCP concentration increased from 25 to 200 fg/mL. In contrast, without the magnet there was no visible positive results, even with 100 pg/mL of VCP. The comparison demonstrated that, beyond the enzyme-based amplification, the magnetic focus can improve the detection sensitivity of our device by more than 4000 times. Compared to that of conventional LFIA systems based on the color of gold nanoparticles (GNPs), the detection sensitivity improved by about 10^6 times.[32,33] Compared to that of the LF systems with an enzymatic reaction to enhance the color signal, the sensitivity improved by 2×10^4 times and did not require a reader.[34]

The quantitative results of purified VCP in PBS buffer is shown in Figure 5. The non-zero value from the blank could be attributed to the background from HRP in the detection zone of the strip and the varying levels of brightness in the images. It can be seen that there is a clear difference in the colorimetric signal between 25 fg/mL and the blank, indicating that the detection can reach a limit as low as 25 fg/mL VCP in PBS. Meanwhile, the quantitative results increased with the concentration of VCP,

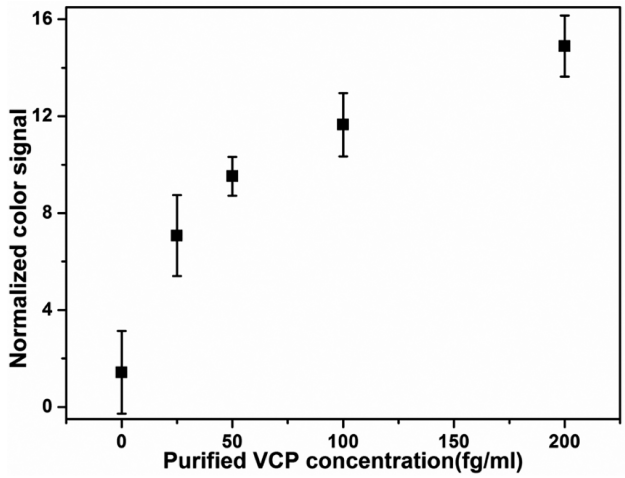

Figure 5. Quantitative results of mLFS detection of purified VCP in 10 mM PBS.

suggesting the quantitative determination of target protein based on the colorimetric signal. Based on the quantitative results shown in Figure 5, the limit of detection was calculated to be 21.82 fg/mL. To further demonstrate the detection capability of mLFS in biological samples, a mixture of proteins extracted from tissue lysate samples were tested for the expression of VCP. After a typical tissue lysis process, the mixed proteins were resuspended in 10 mM PBS. The detection results in Figure 6

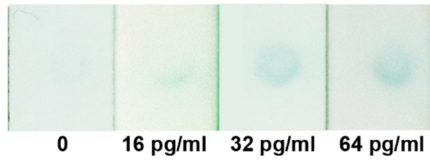

Figure 6. Detection of VCP in mixed proteins extracted from the tissue of cervical cancer patients.

show that VCP could be detected at 16 pg/mL of protein mixtures with naked eyes. Detection of targets in a low amount of protein mixtures extracted from tissues show the potential of the device for a range of applications. With higher concentration of total proteins, the color density of the obtained dots increased. In our previous work, we demonstrated that, with enzymatic-enhanced LFIA, VCP could be recognized at a limit of 28.8 ng/mL of protein mixture extracted from tissue.[36] The results shown in Figure 6 exhibited a marked improvement in sensitivity in clinical samples.

The comparison between detection with and without external magnet in Figure 4 demonstrated a dramatic enhancement in sensitivity due to magnetic focus. To investigate the effect of magnetic focus on the probes at the signal generation zone, SERS and dark-field microscopy was used to directly evaluate the movement and distribution of magnetic probes in the magnetic field. Limited by the nontransparent LF strip, two devices were used to study the flow and distribution of nanoprobes in the microchannel of the NC membrane.

For SERS characterization, a microchannel shown in Figure S2 was fabricated using a glass capillary tube fixed on a glass slide for evaluation of probe behavior by SERS. A conjugate pad is attached to one end of the tube for application of the sample solution, while at the other end an absorbent pad was attached to drive the solution flow through the tube. The corner of the pads

DOI: 10.1021/acs.analchem.8b04848
Anal. Chem. 2019, 91, 2876−2884

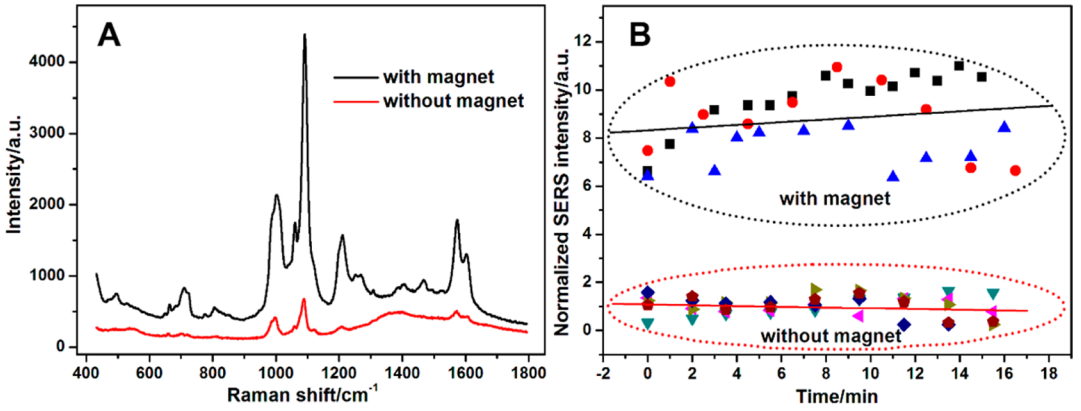

Figure 7. SERS characterization of the magnetic nanoparticles in the microchannel. (A) SERS signal after 15 min of sample addition; (B) normalized SERS intensity of the peak at 1091.5 cm^{-1} with respect to time from the application of solution with magnetic nanoparticles in the microchannel and the corresponding linear fit. Different symbols were from individual measurements.

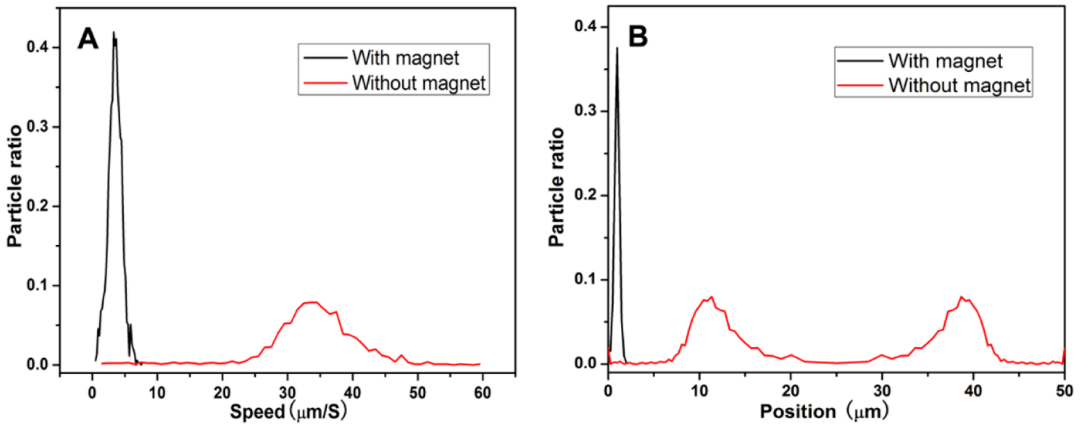

Figure 8. Illustration of the movement and speed distribution of magnetic nanoparticles in the microchannel and the simulated spatial distribution of magnetic nanoparticles along the cross section of the microchannel. *y*-Axis represents the ratio of the number of particles at specific speed (A) or position (B) to the total number of particles in the microchannel.

was in contact with the microchannel for the sample flow. A magnet was fixed to the middle of the capillary tube and the effect of magnetic field on the magnetic probes was tested. The sample solution with gold-coated magnetic nanoparticles modified with a Raman reporter (4-MPy) was applied onto the conjugate pad and the SERS spectra were recorded over time.

After exclusion of the factors contributing to SERS activity change due to the accumulation of probes (as discussed in Figure S3), the SERS intensity of 4-MPy on gold-coated magnetic nanoparticles was used to reveal the number of magnetic nanoparticles. It can be seen in Figure 7A that, after ∼15 min of sample flow, the SERS intensity from the magnetic field focused probes is greater than that from the ones without magnet, indicating that, with magnetic focus, more magnetic probes can be focused at the detection zone. To further characterize the increase in accumulation of gold-coated magnetic nanoparticles with respect to time with and without magnetic field, the time-dependent SERS intensity was also recorded. The plots of normalized SERS intensity of the peak at 1091.5 cm^{-1} with and without magnetic field is illustrated in Figure 7B. A linear fit plotted in Figure 7B reveals that the SERS intensity from samples with magnetic focus was about 7−10 times greater than that without magnetic focus. When characterizing by SERS, it is clear that, with magnetic focus, the movement of the gold-coated magnetic nanoparticles is affected by the magnetic focus and their movement is much slower than that without magnetic focus, resulting in a higher density of gold-coated magnetic nanoparticles at the signal generation site. Consequently, a corresponding higher SERS intensity suggests an increase in concentration of the target labeled with magnetic probes at the signal generation site, depicting an improved capture efficiency and, thus, an enhanced detection sensitivity.

In addition to SERS, dark-field images were recorded to directly demonstrate the movement of magnetic probes in a microchannel due to the magnetic field. The test device was similar to the one used for SERS signal measurement but modified beause the glass capillary showed a strong background from dark-field images. As shown in Figure S4, on the glass slide, wax was applied to form a region of size 5 × 25 mm, similar to the size of the NC membrane on the strip used for detection. Then a cover glass was placed on the glass slide followed by heating to melt the wax and construct a microchannel between the cover glass and glass slide separated with a wax layer. The height of the channel was measured to be about 50 μm. The conjugate pad and absorbent pad were fixed at the end of the channel, respectively, while the magnet was fixed beneath the middle of the channel to evaluate the movement and distribution of the nanoparticle probe influenced by the magnetic focus. The

DOI: 10.1021/acs.analchem.8b04848
Anal. Chem. 2019, 91, 2876−2884

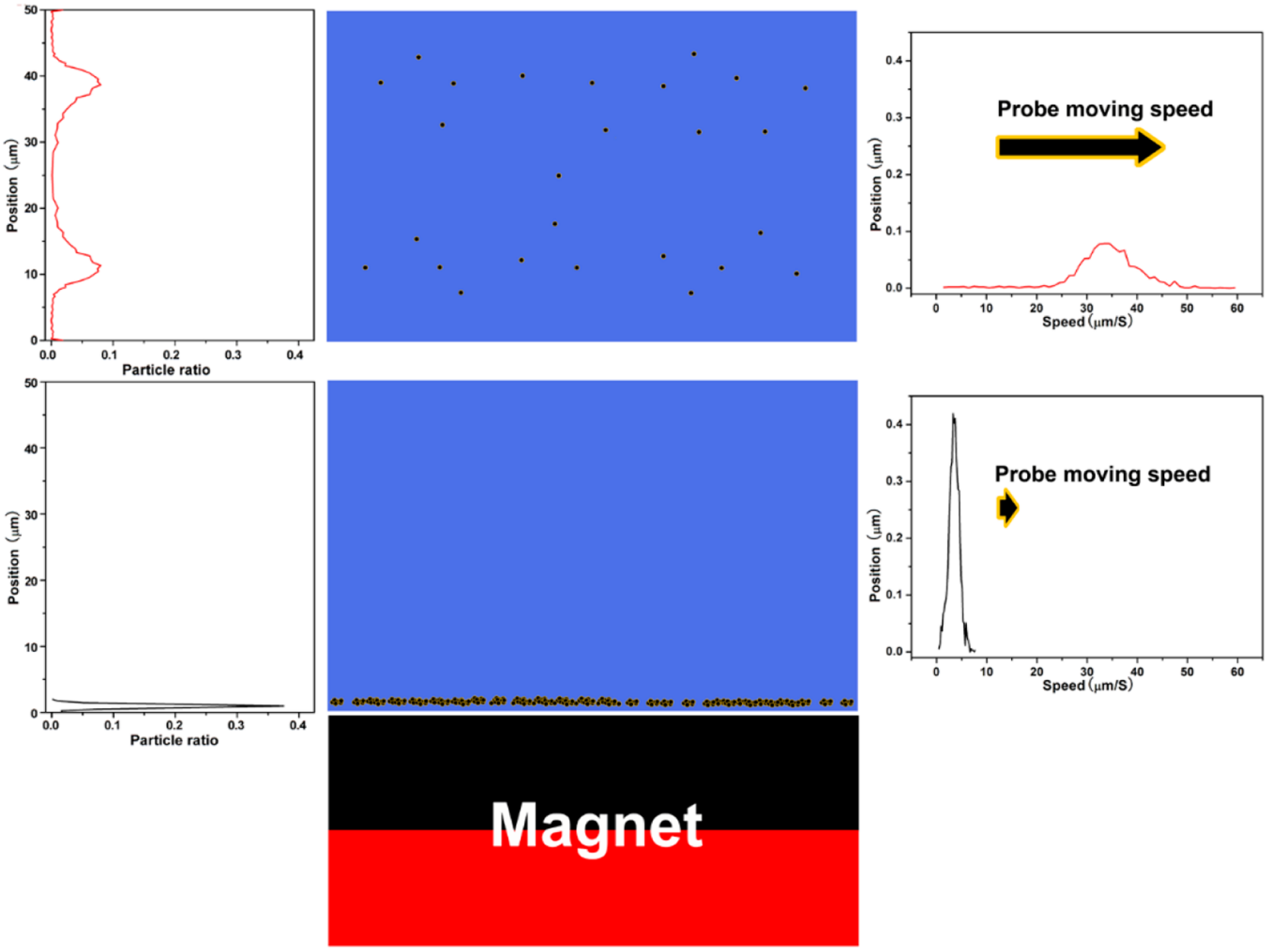

Figure 9. Schematic of magnetic probes in the microchannel. Small dots with black core and golden shell represents magnetic probes. The number, spatial, and speed distribution profile of the magnetic probes are illustrated based on SERS spectra, dark-field imaging, and simulation results.

sample solution was applied onto the conjugate pad to allow the samples to flow through the absorbent pad through the microchannel. The movement of magnetic probes in the channel was recorded by dark-field imaging every 10 s after 2 min of flow initiation (video included as Supporting Information). The first frame of each video is the image of a microruler under the same objective. To better track the magnetic nanoparticles in the images, the exposure time with magnet was kept at 500 ms while for the case without magnet it was kept at 100 ms. Results in the video confirm that the magnetic field reduced the speed at which particles flow through the strip. Without the magnetic field some larger aggregates of magnetic nanoparticles was found to move at speeds similar to the smaller ones, indicating that without magnetic focus the movement of magnetic nanoparticles was primarily driven by capillary flow. Contrastingly, with the magnet it was obvious that some larger aggregates were retained in the same position during measurement and some others moved at a slower rate compared to smaller particles, indicating that the magnetic field tends to reduce the movement of magnetic nanoparticles and this effect became pronounced with larger aggregates. In Figure S4 the magnetic nanoparticles trapped in the magnetic field could be directly noted in the images. To quantify the speed of magnetic nanoparticles, PIV analysis was performed utilizing the dark-field images as input data. Figure 8A shows the speed of movement of magnetic nanoparticles in the microchannel. The difference in the speed of magnetic nanoparticles with and without magnetic focus was noted. The peaks of the speed distribution were 3.3 and 33.5 μm/s respectively for conditions with and without the magnetic field, rendering a tenfold difference in speed due to the magnetic focus which could result in an increase in the density of magnetic nanoparticles in the detection zone of LF strip. Furthermore, the tenfold reduction in speed enabled a prolonged interaction which is tenfold longer than the interaction time between the magnetic probe-labeled targets and the antibodies immobilized at the detection zone during mLFS.

The spatial distribution of magnetic nanoparticles in the test was simulated for conditions with/without magnetic field. In Figure 8B, the position of x-axis represents the distance from the wall of the microchannel in the cross section, from a value of 0 at one side to 50 μm at the other side. It can be seen that the magnetic nanoparticles were concentrated at the wall of the microchannel where the magnet was fixed, while for conditions without the magnet, the magnetic nanoparticles mostly distributed in specific regions away from the walls of the microchannel because of the effect of "tubular pinch" phenomena.[43] Simulation results in Figure 8B show the distribution of the magnetic probe-labeled targets in the microchannels constructed by the pores of the NC membrane

DOI: 10.1021/acs.analchem.8b04848
Anal. Chem. 2019, 91, 2876−2884

in the detection zone of the LF strip. According to the simulation, magnetic focus could concentrate all the probes in the region 2 μm from the wall, while without the magnetic focus only 1.5% of the probes were found in the same region. It is reported that the capture efficiency of conventional LFIA is less than 1%.[31] Thus, although the magnetic focus would influence the distribution of probes in the vertical direction of the LF strip and part of the antibodies in the detection zone may not be occupied by the target, the distribution of magnetic probe-captured target in the microchannels could still contribute to improved sensitivity.

Figure 9 illustrates the effect of magnetic focus on the movement of nanoparticles. The cross section of the microchannel is represented by a blue square, while the magnetic probes are depicted by small circles with a black core and gold shell. From the SERS results, the number of magnetic nanoparticles in the magnetic field was estimated to be seven- to tenfold greater than that without magnet. The PIV analysis based on dark-field images indicated a tenfold reduction in the movement of magnetic probes due to the magnetic field compared to those without magnet. Simulation results indicated that the magnetic field could concentrate the probes near the walls of the microchannel where antibodies were immobilized to improve capture efficiency to result in increased sensitivity.

CONCLUSION

In this work, we present a unique mFLS platform based on the magnetic focus concept for ultrasensitive detection of protein biomarkers by colorimetry while retaining the simplicity of the lateral flow device. We show that a cervical cancer protein biomarker, VCP, could be detected at a concentration as low as 25 fg/mL in PBS. We further show that quantification is possible in the 200 fg/mL range. The sensor was further tested by analyzing tissue samples, where VCP could be detected in 16 pg/mL protein mixtures extracted from tissues of cervical cancer patients. We validate the enhanced particle accumulation and target capture concept with magnetic focus in LF device by SERS, dark-field imaging, and PIV simulation. The proposed mLFS strategy could be extended to detect a variety of other protein biomarkers and most crucially has the potential to take POC immunoassays to the ultrasensitive regime to enable the detection of rare events by naked eye color monitoring.

ASSOCIATED CONTENT

Supporting Information

The Supporting Information is available free of charge on the ACS Publications website at DOI: 10.1021/acs.analchem.8b04848.

Images of mLFS detection results from blank and 100 fg/mL VCP with different amounts of HRP; images of simulated device for SERS characterization; SERS characterization of magnetic nanoparticles concentrated with external magnet; image of simulated device for dark-field imaging characterization. (PDF)

Animation of the magnetic probe movement in the channel with and without external magnet recorded by dark-field imaging every 10 seconds after 2 min of flow initiation. Video (AVI)

Video (AVI)

AUTHOR INFORMATION

Corresponding Author

*E-mail: jirudaya@illinois.edu.

ORCID

Wen Ren: 0000-0002-8712-190X

Joseph Irudayaraj: 0000-0002-0630-1520

Notes

The authors declare no competing financial interest.

ACKNOWLEDGMENTS

This research is supported by the U.S. Department of Agriculture, Agricultural Research Service, under Project No. 8072-42000-077. Any opinions, findings, conclusion, or recommendations expressed in this publication are those of the author(s) and do not necessarily reflect the view of the U.S. Department of Agriculture. Support from the Purdue Center for Cancer Research NIH grant P30 CA023168 is appreciated.

REFERENCES

(1) Li, Z. H.; Wang, Y.; Wang, J.; Tang, Z. W.; Pounds, J. G.; Lin, Y. H. *Anal. Chem.* **2010**, *82*, 7008−7014.

(2) Anfossi, L.; D'Arco, G.; Calderara, M.; Baggiani, C.; Giovannoli, C.; Giraudi, G. *Food Addit. Contam., Part A* **2011**, *28*, 226−234.

(3) Cho, I. H.; Bhunia, A.; Irudayaraj, J. *Int. J. Food Microbiol.* **2015**, *206*, 60−66.

(4) Cho, I. H.; Irudayaraj, J. *Anal. Bioanal. Chem.* **2013**, *405*, 3313−3319.

(5) Lee, S.; Mehta, S.; Erickson, D. *Anal. Chem.* **2016**, *88*, 8359−8363.

(6) Hwang, S. G.; Ha, K.; Guk, K.; Lee, D. K.; Eom, G.; Song, S.; Kang, T.; Park, H.; Jung, J.; Lim, E.-K. *Sci. Rep.* **2018**, *8*, 12999.

(7) Corstjens, P.; De Dood, C. J.; Kornelis, D.; Fat, E. T. K.; Wilson, R. A.; Kariuki, T. M.; Nyakundi, R. K.; Loverde, P. T.; Abrams, W. R.; Tanke, H. J.; Van Lieshout, L.; Deelder, A. M.; Van Dam, G. J. *Parasitology* **2014**, *141*, 1841−1855.

(8) Li, J.; Macdonald, J. *Lab Chip* **2016**, *16*, 242−245.

(9) Panferov, V. G.; Safenkova, I. V.; Varitsev, Y. A.; Drenova, N. V.; Kornev, K. P.; Zherdev, A. V.; Dzantiev, B. B. *Talanta* **2016**, *152*, 521−530.

(10) Leung, W.; Chan, C. P.; Rainer, T. H.; Ip, M.; Cautherley, G. W.; Renneberg, R. *J. Immunol. Methods* **2008**, *336*, 30−36.

(11) Jarvis, J. N.; Percival, A.; Bauman, S.; Pelfrey, J.; Meintjes, G.; Williams, G. N.; Longley, N.; Harrison, T. S.; Kozel, T. R. *Clin. Infect. Dis.* **2011**, *53*, 1019−1023.

(12) Vaidya, V. S.; Ford, G. M.; Waikar, S. S.; Wang, Y. Z.; Clement, M. B.; Ramirez, V.; Glaab, W. E.; Troth, S. P.; Sistare, F. D.; Prozialeck, W. C.; Edwards, J. R.; Bobadilla, N. A.; Mefferd, S. C.; Bonventre, J. V. *Kidney Int.* **2009**, *76*, 108−114.

(13) Xing, C. R.; Liu, L. Q.; Song, S. S.; Feng, M.; Kuang, H.; Xu, C. L. *Biosens. Bioelectron.* **2015**, *66*, 445−453.

(14) Zou, Z. X.; Du, D.; Wang, J.; Smith, J. N.; Timchalk, C.; Li, Y. Q.; Lin, Y. H. *Anal. Chem.* **2010**, *82*, 5125−5133.

(15) Choi, J. R.; Hu, J.; Tang, R. H.; Gong, Y.; Feng, S. S.; Ren, H.; Wen, T.; Li, X. J.; Wan Abas, W. A.; Pingguan-Murphy, B.; Xu, F. *Lab Chip* **2016**, *16*, 611−621.

(16) O'Farrell, B. In *The Immunoassay Handbook*, 4th ed.; Elsevier: Oxford, 2013; pp 89−107.

(17) Bahadır, E. B.; Sezgintürk, M. K. *TrAC, Trends Anal. Chem.* **2016**, *82*, 286−306.

(18) Hossain, S. M. Z.; Ozimok, C.; Sicard, C.; Aguirre, S. D.; Ali, M. M.; Li, Y. F.; Brennan, J. D. *Anal. Bioanal. Chem.* **2012**, *403*, 1567−1576.

(19) Kim, C.; Yoo, Y. K.; Han, S. I.; Lee, J.; Lee, D.; Lee, K.; Hwang, K. S.; Lee, K. H.; Chung, S.; Lee, J. H. *Lab Chip* **2017**, *17*, 2451−2458.

(20) Xu, H.; Mao, X.; Zeng, Q. X.; Wang, S. F.; Kawde, A. N.; Liu, G. D. *Anal. Chem.* **2009**, *81*, 669−675.

DOI: 10.1021/acs.analchem.8b04848
Anal. Chem. 2019, 91, 2876−2884

(21) Yen, C.-W.; de Puig, H.; Tam, J. O.; Gómez-Márquez, J.; Bosch, I.; Hamad-Schifferli, K.; Gehrke, L. *Lab Chip* **2015**, *15*, 1638−1641.
(22) Anfossi, L.; Di Nardo, F.; Giovannoli, C.; Passini, C.; Baggiani, C. *Anal. Bioanal. Chem.* **2013**, *405*, 9859−9867.
(23) Rajendran, V. K.; Bakthavathsalam, P.; Ali, B. M. J. *Microchim. Acta* **2014**, *181*, 1815−1821.
(24) Juntunen, E.; Arppe, R.; Kalliomaki, L.; Salminen, T.; Talha, S. M.; Myyrylainen, T.; Soukka, T.; Pettersson, K. *Anal. Biochem.* **2016**, *492*, 13−20.
(25) Zeng, Q.; Mao, X.; Xu, H.; Wang, S.; Liu, G. *Am. J. Biomed. Sci.* **2009**, *1*, 70−79.
(26) Kumar, R.; Singh, C. K.; Kamle, S.; Sinha, R. P.; Bhatnagar, R. K.; Kachru, D. N. *Food Chem.* **2010**, *122*, 1298−1303.
(27) Rivas, L.; Medina-Sanchez, M.; de la Escosura-Muniz, A.; Merkoci, A. *Lab Chip* **2014**, *14*, 4406−4414.
(28) Tang, R.; Yang, H.; Gong, Y.; Liu, Z.; Li, X.; Wen, T.; Qu, Z.; Zhang, S.; Mei, Q.; Xu, F. *Sci. Rep.* **2017**, *7*, 1360.
(29) Rosenfeld, T.; Bercovici, M. *Lab Chip* **2014**, *14*, 4465−4474.
(30) Moghadam, B. Y.; Connelly, K. T.; Posner, J. D. *Anal. Chem.* **2014**, *86*, 5829−5837.
(31) Moghadam, B. Y.; Connelly, K. T.; Posner, J. D. *Anal. Chem.* **2015**, *87*, 1009−1017.
(32) Byzova, N. A.; Smirnova, N. I.; Zherdev, A. V.; Eremin, S. A.; Shanin, I. A.; Lei, H.-T.; Sun, Y.; Dzantiev, B. B. *Talanta* **2014**, *119*, 125−132.
(33) Mao, X.; Wang, W.; Du, T.-E. *Sens. Actuators, B* **2013**, *186*, 315−320.
(34) Parolo, C.; de la Escosura-Muñiz, A.; Merkoçi, A. *Biosens. Bioelectron.* **2013**, *40*, 412−416.
(35) Ren, W.; Cho, I.-H.; Zhou, Z.; Irudayaraj, J. *Chem. Commun.* **2016**, *52*, 4930−4933.
(36) Mohammed, S. I.; Ren, W.; Flowers, L.; Rajwa, B.; Chibwesha, C. J.; Parham, G. P.; Irudayaraj, J. M. K. *Oncotarget* **2016**, *7*, 18787−18797.
(37) Unal, B.; Durmus, Z.; Kavas, H.; Baykal, A.; Toprak, M. S. *Mater. Chem. Phys.* **2010**, *123*, 184−190.
(38) Zhou, Z.; Irudayaraj, J. *Analyst* **2015**, *140*, 938−944.
(39) Tamer, U.; Gundogdu, Y.; Boyaci, I. H.; Pekmez, K. *J. Nanopart. Res.* **2010**, *12*, 1187−1196.
(40) Haiss, W.; Thanh, N. T.; Aveyard, J.; Fernig, D. G. *Anal. Chem.* **2007**, *79*, 4215−4221.
(41) Adrian, R. J.; Yao, C.-S. *Appl. Opt.* **1985**, *24*, 44−52.
(42) Meinhart, C. D.; Wereley, S. T.; Gray, M. H. B. *Meas. Sci. Technol.* **2000**, *11*, 809−814.
(43) Cao, J.; Wereley, S. In *Proceedings of the ASME International Mechanical Engineering Congress and Exposition*, Anaheim, CA, 2004; ASME: New York, 2004; pp 243−252.
(44) Wang, X.; Cui, Y.; Irudayaraj, J. *ACS Nano* **2015**, *9*, 11924−11932.
(45) Lee, K.; Cui, Y.; Lee, L. P.; Irudayaraj, J. *Nat. Nanotechnol.* **2014**, *9*, 474−480.

DOI: 10.1021/acs.analchem.8b04848
Anal. Chem. 2019, 91, 2876−2884